THE JOURNAL OF PHYSICAL CHEMISTRY Letters

Letter

Cite This: J. Phys. Chem. Lett. 2018, 9, 1415−1421

pubs.acs.org/JPCL

Self-Assembly of Janus Nanoparticles into Transformable Suprastructures

Chengjun Kang[†] and Andrei Honciuc*[,†]

[†]Institute of Chemistry and Biotechnology, Zurich University of Applied Sciences, Einsiedlerstrasse 31, 8820 Waedenswil, Switzerland

Supporting Information

ABSTRACT: One of the greatest challenges in colloidal self-assembly is to obtain multiple distinct but transformable suprastructures from the same particles in monophasic solvent. Here, we combined deformable and rigid lobes in snowman-shaped amphiphilic Janus nanoparticles (JNPs). These JNPs exhibited excellent ability to self-assemble into micelles, worms, mini-capsules, giant- and elongated-vesicles. This rich suprastructural diversity was obtained by kinetic manipulation of the self-assembly conditions. The suprastructures consist of four to thousands of highly oriented JNPs with dimensions ranging from 500-nanometer to 30-μm. Moreover, the suprastructures can be transformed into one another or dissembled into individual particles. These features make colloidal assembly highly comparable to that of amphiphilic molecules, however, key differences were discovered.

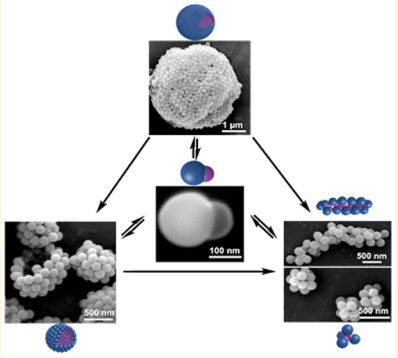

Colloidal assembly has aroused great interest due to its applications in photonics,[1,2] (bio)sensing[3,4] and catalysis.[5] Because of some similarities, colloidal assembly has often been compared with molecular self-assembly.[6−11] Translating molecular self-assembly behavior to colloidal-sized building blocks could be useful in developing novel material with new functionalities.[12−14] Although significant progress has been made in the past decade,[9,10] with examples including trimers,[15] microcapsules,[16] simple spherical micelles assembled from micron-sized Janus particles,[17,18] fibrillar triple helices,[19] and kagome lattice[20] obtained respectively from di- and triblock hard spherical microparticles, colloidal self-assembly remains far less versatile when compared to that of molecules. For instance, it is well-known that one type of molecular amphiphiles can be self-assembled into different suprastructures as micelles, worms, and vesicles.[21,22] Additionally, the molecular suprastructures are transformable, e.g., vesicles can be transformed into worms and micelles,[23,24] and such properties have not been yet reported in colloidal assemblies. Here, we show that the same specially designed snowman-shaped Janus nanoparticles[25,26] can indeed self-assemble into multiple distinct suprastructures, such as micelles, worms, mini-capsules, giant- and elongated-vesicles constituted of highly oriented JNPs. Even more, the obtained supracolloidal structures can reversibly transform into each other.

In the present work, we used poly(*tert*-butyl acrylate)-poly(3-(triethoxysilyl)propyl-methacrylate (PtBA-PTPM) JNPs, which were synthesized by seeded emulsion polymerization[27] (Figure 1). Mildly cross-linked PtBA NP (140 ± 7 nm in diameter) was used as seed along with phase separation of 3-(triethoxysilyl)-propyl-methacrylate (TPM) under surfactant-free conditions in gram scale amount. The resulting PTPM lobe had a diameter of 210 ± 9 nm, while the diameter of the PtBA lobe remained the same as the PtBA seed NP (Figure S1). The general JNPs design concept was that the segregation of polar and nonpolar lobes drives the self-assembly. One essential requirement is that the interparticle attractive force can be tuned by altering solvent composition so as to favor different suprastructures. The nonpolar PtBA lobe fulfills this requirement, because its hydrophobic attraction (water contact-angle (CA) 122 ± 5°, Figure S2) can hold together assembled structures. Additionally, this inter-PtBA lobe "colloidal bond"[16] is reversible, and the bonding strength is proportional to the contact area, which depends on the PtBA lobe deformability. On the other hand, PTPM was selected because of its relative hydrophilicity (water CA 54 ± 6°, Figure S2). Also, thanks to the polycondensation of siloxane groups and the resulting high cross-linking degree,[27] the PTPM lobe is rather rigid and able to mechanically support assembled 3D structures.

The self-assembly of PtBA-PTPM JNPs was carried out under shear in ethanol/water mixed solvent. Different suprastructures can be obtained by altering several key parameters. The first parameter is ethanol concentration (volume %) (Figure 2a). Other parameters as JNPs concentration (10.0 mg/mL), mechanical vortex sheering speed (3000 rpm) and temperature (24 °C) were kept constant. No self-assembly was observed in pure water, and self-assembled structures began to appear with the ethanol concentration as little as 1%. The first self-assembled structures were micelles, consisting of 4 to 12 oriented JNPs with the PTPM lobes pointing toward aqueous solution, while the PtBA lobes closely packed together (Figure 2d, Figure S3). By increasing the ethanol amount to 3%, mini-

Received: January 22, 2018
Accepted: March 6, 2018
Published: March 6, 2018

DOI: 10.1021/acs.jpclett.8b00206
J. Phys. Chem. Lett. 2018, 9, 1415−1421

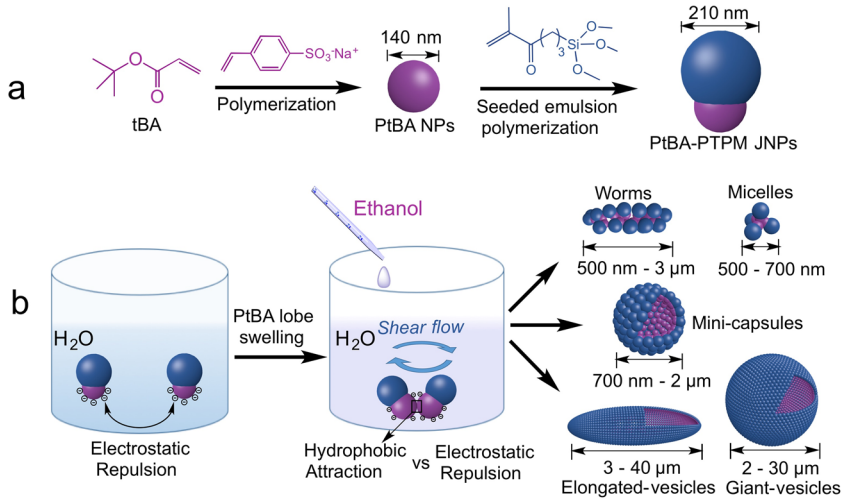

Figure 1. Synthesis and self-assembly of PtBA-PTPM JNPs. (a) Synthesis of PtBA-PTPM JNPs. (b) Self-assembly of PtBA-PTPM JNPs into various suprastructures under shear.

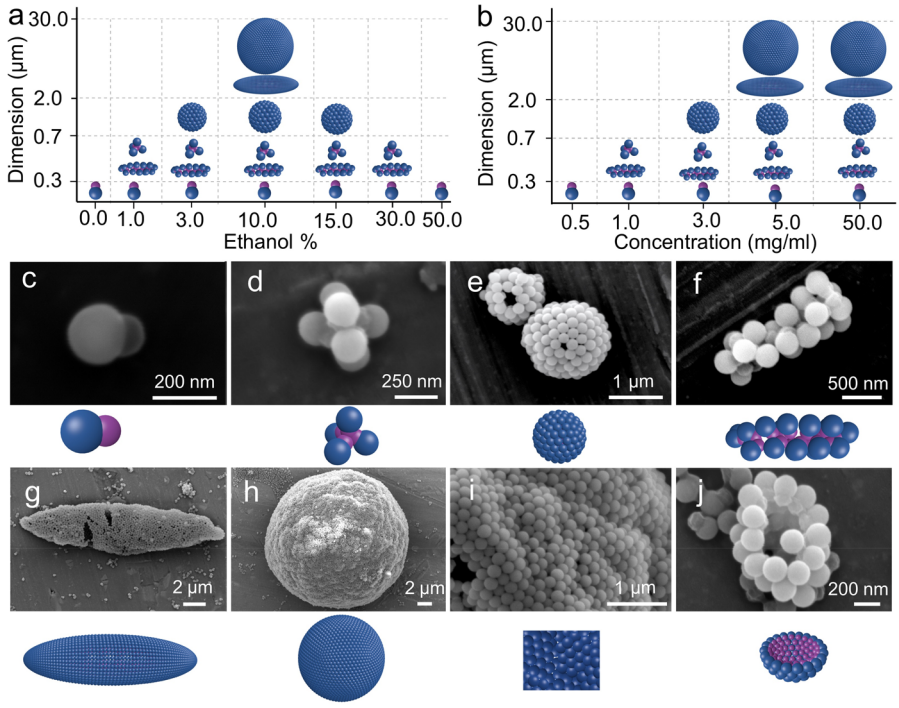

Figure 2. Self-assembly of PtBA-PTPM JNPs under mechanical vortex sheering. (a,b) Influence of ethanol concentration (a) and particle concentration (b) on the self-assembly. Typical SEM images of JNP (c), micelle (d), mini-capsule (e), worm (f), elongated vesicle (g), giant-vesicle (h), surface structure of giant vesicle (i), and open mini-capsule (j). Cartoons depict the most likely assembled structures. (See Supporting Information for suprastructures of different sizes.)

spherical capsules containing about 30 to 100 highly oriented JNPs were obtained (Figure 2e, Figure S4). Their dimensions range from 700 nm to 2 μm. Open mini-capsules (Figure 2j, Figure S5) show that they are composed of hexagonally packed JNP monolayers with the PTPM lobes uniformly oriented toward the outer shell. Theoretically, the maximum size of the mini-capsule is restricted by the JNP geometry and calculated to be 1.1 μm (Figure S6), which is reasonable as compared to the experimental results regarding the slight JNPs size fluctuation. Another interesting finding is the worm-like micelle formed by colloidal particles with anisotropic geometries (Figure 2f, Figure S3). Wormlike micelles have been seen in molecular amphiphiles for decades, however, their detailed structures, such as molecular units arrangement and orientation, have not been directly observed.[28] Here, we can clearly see that worms are elongated structures with oriented rows of JNPs running parallel to their long axis. Considering the large aspect ratio and high flexibility, it is no surprising that the worms in our case do not have crystalline structures as fibrillar triple helices,[19] which will make worms fragile and easily broken into pieces by shear force.

Giant-vesicles with dimensions ranging from 2 to 30 μm were observed at 10% ethanol concentration (Figure 2h, Figure S4). It is difficult to count the precise number of JNPs contained in the giant-vesicles; an approximate calculation (see Supporting Information) indicates that a 30 μm vesicle contains

DOI: 10.1021/acs.jpclett.8b00206
J. Phys. Chem. Lett. 2018, 9, 1415−1421

about 8×10^4 JNPs. Such large vesicles can be observed *in situ* by optical microscope. By adding a fluorescent dye in the aqueous phase, we observed that water is present inside of the suprastructures. Because the fluorescent signal intensity is uniform inside and outside of the vesicles (Figure S4k,l), we conclude that air bubbles did not contribute as a template to the formation of the observed self-assembled suprastructures.

Broken vesicles show that they are composed of a monolayer JNPs with the PTPM lobes pointing outward (Figure S5). The typical lipid bilayer structures of molecular vesicles[29] were not observed. This could be explained by the rigid geometries of JNPs, which, unlike molecular surfactants, can only allow the curvature bending from the larger PTPM lobe toward the smaller PtBA lobe. The giant-vesicles can be spherical or elongated (Figure 2g). It is rather surprising that these single-layer JNPs formed giant structures survived from the capillary forces during drying for SEM measurement,[30] which implies their considerable mechanical stability, likely due to a tight packing of JNPs. Due to higher adhesion energies, the suprastructures with tightly packed JNPs are likely those that have survived shearing forces. While the shear forces are necessary for the JNPs to come together and overcome the electrostatic repulsion, the same shear forces may also lead to the destruction of the loosely packed structures. In addition, the curvature (1/radius) of giant-vesicles is significantly lower than that required by the JNP geometry as seen in mini-capsules. A detailed examination reveals the giant-vesicle walls are made by highly oriented and hexagonally packed JNPs domains. Each domain has a curvature comparable to that of mini-capsules by slightly shifting in their arrangements, forming wave-like structures on the vesicle surface and removing the restrictions of the JNPs geometry on the vesicle size. The relaxation of the geometric restrictions with respect to curvature can be rationalized by the existence of the packing defects at the boundary of closely packed JNP domains, which can be clearly observed from the magnified SEM images of the concave parts of the wavy vesicle walls (Figure S4i). The orientation of the loosely packed JNPs at the boundary of the closely packed domains is still preserved, namely with the PtBA lobe pointing inside the vesicle (Figure S4i and Figure S5f). From the calculation in Figure S6, we find that this size limit due to curvature restrictions is around 1.1 μm, much smaller that the giant vesicles (as big as 20 μm). Therefore, the existence of packing defects at the boundary of closely packed domains is the only way that single layered giant vesicles can become so large, namely, by relaxation of the geometric restrictions through the wavelike structuring of the walls. The cartoon presented in Figure S7 depicts this situation.

Such wavelike single-walled structures have no known molecular equivalent to date. Further increase in the ethanol concentration to 15%, and a decrease in the sizes of self-assembled structures were observed. No self-assembled structure was detected when the ethanol concentration exceeded 50%.

The ethanol amount has significant influence on the JNPs self-assembly, as it can swell the PtBA lobes and enhance their deformability. By preparing colloidal crystal from PtBA seed particles, we calculated the swelling factors 2.1, 1.5, and 1.1 times corresponding to the ethanol concentrations of 100%, 10% and 1% in water (Figure S8). The swelling of the PtBA NPs was further confirmed by the dynamic light scattering (DLS) measurement, which shows that PtBA NPs swelled around 1.4 times in 10% ethanol (Figure S9). Due to size change and swelling, it is possible that some degree of deformation during the self-assembly may occur. Assuming that the lobes are perfectly elastic, by tuning the deformability, the inter-PtBA lobe contact area and hydrophobic attraction strength as well as the structural stability of the suprastructures can be controlled. Simple estimation on the adhesion energy between the PtBA lobes (assuming they are elastically deformable) may help us to understand the role of deformability in the present study. The free energy of hydrophobic interaction between of two surfaces in liquid can be calculated as follows:[31]

$$E_{\text{attractive}} = -2A\gamma_{\text{SL}} \tag{1}$$

where A is the area of the contact between the two lobes and γ_{SL} is the interfacial energy. Taking the surface tension of water with 10% ethanol 47.53 mN/m[32] and surface energy of the PtBA polymer 30.5 mN/m,[33] γ_{SL} is ≈2 mN/m ($\gamma_{SL} = \gamma_S + \gamma_L - 2\sqrt{\gamma_S\gamma_L}$). Next, we calculate the lower and the upper limit of the free energy of hydrophobic interaction between PtBA lobes in contact, which is determined by the contact area A in the absence of deformation and in case of extreme deformation, respectively. First, in the absence of deformation, the PtBA lobes form a point contact and A_{min} is set by all the points on the surface of the contacting lobes within 1.5−2 nm separation distance, i.e., the effective length of the hydrophobic interaction.[31] The obtained A_{min} = 436.5 nm^2, corresponding to a minimum adhesive energy of E_{min} = −1746 pN·nm, or −426 kT (1 kT = 4.1 pN·nm). In fact, −426 kT is not large for particles of this size, considering that the adsorption energies of the comparable size JNPs at heptane/water interface, is as large as 60000 kT.[34] At short-range, strong attraction force is needed to overcome the electrostatic repulsion. The energy of electrostatic repulsion between two JNPs was calculated to be ≈355 kT and 345 kT at a separation distances of 1 and 20 nm respectively, with the latter value being well beyond the effective range of hydrophobic interaction. The need for external energy input through mechanical stirring thus becomes evident. The energy of electrostatic interaction was calculated with the formula:[31]

$$E_{\text{repulsive}} = 0.5R\left[64\pi\varepsilon_0\varepsilon\left(\frac{kT}{e}\right)^2 \tan h^2\left(\frac{e\psi}{4kT}\right)\right] \times \exp(-\Lambda D) \tag{2}$$

where ε is the electric permittivity of vacuum (8.86×10^{-12} C^2 J^{-1} m^{-1}), ε_0 is the relative permittivity of water with 10% ethanol (≈75), e is the elementary charge (1.62×10^{-19} C), ψ − zeta potential (-56.5×10^{-3} V), T = 298 K, R is the hydrodynamic radius of the JNP measured by DLS (1.4×10^{-7} m), $1/\Lambda$ is the Debye length (9.6×10^{-7} m for pure water),[31] and D is the separation distance.

In addition to overcoming electrostatic repulsion, the shear conditions in the assembly experiments also require strong adhesion forces to hold the assembled structures together and prevent being torn apart. Under these considerations, increased contacting area due to slight deformation of the PtBA lobes may lead strengthening the adhesives contact thus provide sufficient attraction energy to realize assembly. The upper limit of the free energy of hydrophobic interaction is set by the maximum contact area between PtBA lobes that could be as large as πR^2 (R is the radius of the PtBA lobe), or 15166 nm^2, thus the free energy of hydrophobic interaction $E_{\text{max}} \sim$ 60600 kT. To further test this hypothesis, we synthesized amphiphilic

DOI: 10.1021/acs.jpclett.8b00206
J. Phys. Chem. Lett. 2018, 9, 1415−1421

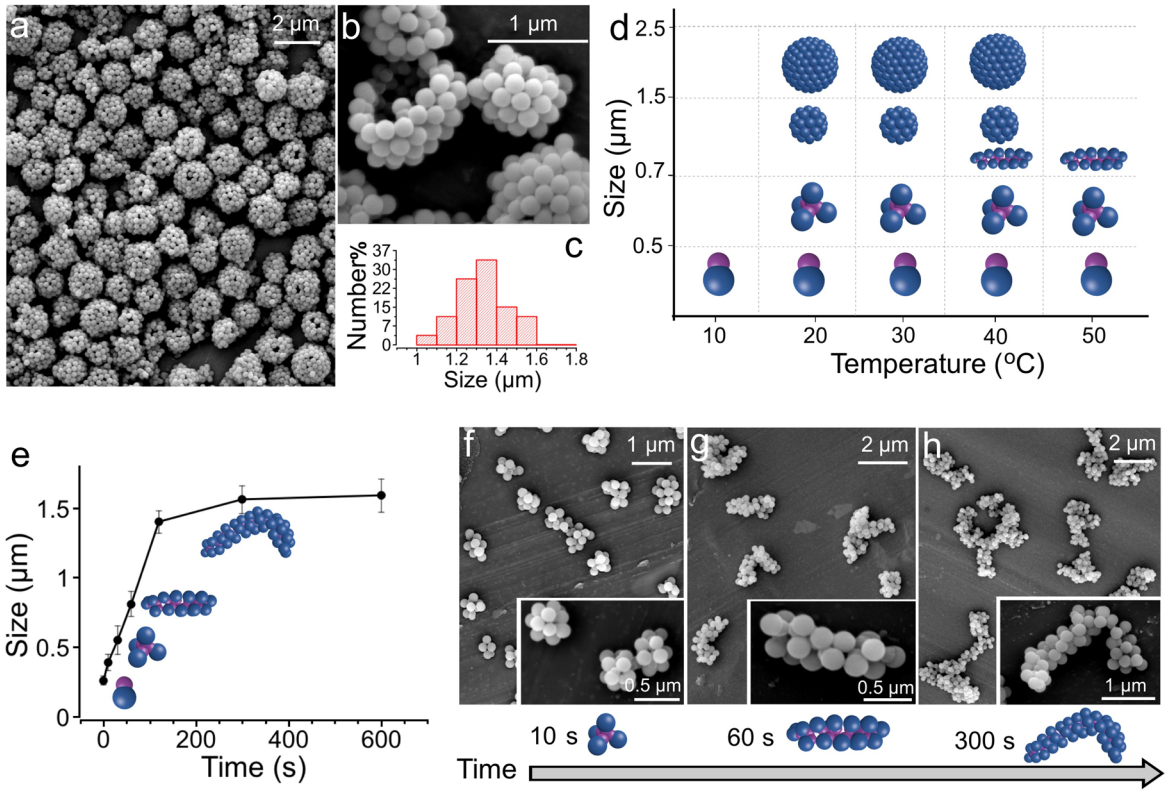

Figure 3. Self-assembly of PtBA-PTPM JNPs under sonication. (a) Mini-capsules obtained at 24 °C. (b) An open mini-capsule of panel a, showing the JNPs orientation and void interior. (c) Diameter distribution of the mini-capsules (a). (d) Dependence of the self-assembled structures on the sonication temperature. The sonication time was 25 min. (e) The assembled structure size, measured by DLS in situ, plotted as a function of sonication time. The sonication temperature was 50 °C. SEM images of micelles (f) and worms (g,h) taken from the different time points of the plot in panel e. The inset shows detailed structures of micelles and worms. Cartoons depict the most likely assembled structures.

JNPs PTPM−polystyrene (PTPM−PS) (Figure S10), which has very similar size, geometry, and zeta potential with the PTPM-PtBA JNPs. However, the PS lobe as observed in Figure S10 cannot be swelled by ethanol and thus remains rigid, we did not observe any assembly for PTPM−PS JNPs under any conditions. Based on this evidence, it is likely that the lobe deformability plays an important role in the assembly.

Broken capsules show that the PtBA lobe surfaces are rather rough and wrinkled in aggregates (Figure 2j), in sharp contrast to the smooth surfaces prior to assembly (Figure 2c). This roughening of the lobe surface is likely a result of buckling due to the capillary forces upon drying after the PtBA swells significantly at higher ethanol concentrations.

The hydrophobic interaction between the PtBA lobes is the main attraction force that holds the self-assembled aggregates together, and this hypothesis was experimentally proved by converting hydrophobic *tert*-butyl groups in the PtBA lobe into hydrophilic hydroxyl groups. The formed poly(*N*-(2-hydroxyethyl) acrylamide)−PTPM (PHEA−PTPM) JNPs (Figure S11) share very similar geometries and zeta potentials with the PtBA−PTPM JNPs, however, no PHEA−PTPM JNPs self-assembly was observed under any conditions. Therefore, the role of ethanol in the JNPs self-assembly can be understood as follows: no self-assembly was observed when the ethanol concentration was below 1%, because the limited swelling degree can only provide small interaction areas between the PtBA lobes, and the resulting weak hydrophobic attraction is insufficient to hold JNPs together. Adding a small amount of ethanol swells the PtBA lobe. The higher deformability and enlarged contacting area result in an increased attraction force; therefore, JNPs self-assembled into micelles. The same rationale applies to the formation of mini-capsules and giant-vesicles. However, excessive ethanol addition, ≫ 15%, resulting in a serious decrease in solvent polarity and weaken the inter-PtBA lobe hydrophobic attractions. JNPs can be fully dispersed in 50% ethanol/water, and no self-assembly was observed (Figure 2a).

Concentration is an important parameter for the self-assembly of amphiphilic molecules. However, it is surprising that this parameter has largely been overlooked in the colloidal self-assembly. Even though Chris et al.[16] observed that microcapsules can only be formed under high particle concentrations, a detailed study about the influence of concentration on colloidal self-assembly has not been reported yet. The next parameter we used to control colloidal self-assembly is JNP concentration (Figure 2b), with ethanol concentration (10%), temperature (24 °C), and mechanical agitation speed (3000 rpm) kept constant. No self-assembled structures were observed at a concentration below 0.5 mg/mL. Above 1.0 mg/mL, micelles were observed. Analogue to molecular amphiphiles, one can name this particular concentration (1.0 mg/mL) at which micelles can be observed as the Janus-critical micelle concentration (J-CMC). We observed mini-capsules at 3.0 mg/mL, and giant-vesicles were formed between 5.0 and 50.0 mg/mL (Figure 2b). Larger concentrations were tried, but particle dispersibility became problematic. It is evident that higher JNPs concentration favors more complex assemblies within a certain concentration range.

Mechanic shearing is the third parameter employed to control the JNPs self-assembly. In order to realize self-assembly,

DOI: 10.1021/acs.jpclett.8b00206
J. Phys. Chem. Lett. 2018, 9, 1415−1421

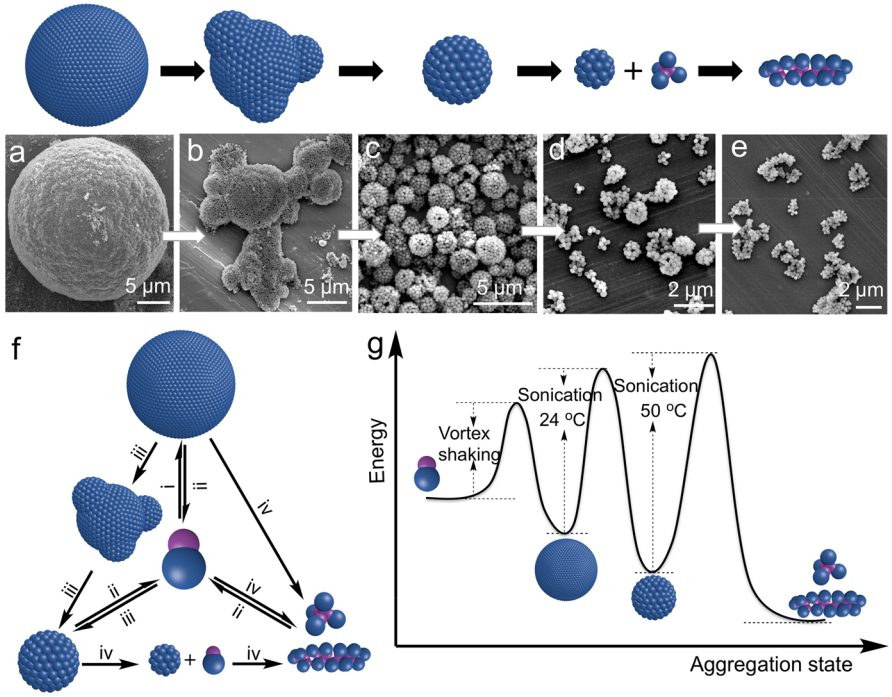

Figure 4. Transformations between different suprastructures. (a–e) Transformations from giant vesicles (a), to multichambered vesicles (b), to mini-capsules (c), to the mixture of micelles and mini-capsules (d), and to worms (e). (f) Full overview of the suprastructural transformations: (i) self-assembly of JNPs into giant- and elongated-vesicles; (ii) disassembly of suprastructures into individual JNPs; (iii) transformation of giant-capsules into multichambered capsules and subsequently into mini-capsules; (iv) formation of micelles and worms. (g) Experiment-based qualitative plot of the energy levels and activation energy barriers of different suprastructures. Cartoons depict the most likely assembled structures.

JNPs must approach each other closely enough to experience hydrophobic attractions. Mechanic shearing can accelerate JNPs motion and provide kinetic energy to overcome electrostatic repulsion barriers, so as to increase interparticles collision probability and accelerate the self-assembly process. In the absence of mechanic shearing, no self-assembly was observed in the present study. On the other hand, mechanic shearing can tear assembled structures apart, consequently, different mechanic shearing will result in different self-assembled equilibrium structures.[35] Therefore, in addition to the shear flow produced by vortex agitation as above, we have further examined JNPs self-assembly under the shear forces of sonication. Based on the previous experiments, we fixed ethanol concentration (10%), JNP concentration (10.0 mg/mL), temperature (24 °C), sonotrode diameter (13 mm), vibration frequency (20 kHz), and amplitude (73.7 μm). Under these conditions, we obtained mini-capsules with remarkably uniform sizes after 10 min sonication (Figure 3a,b). The SEM image shows a large amount of mini-capsules tightly arranged together, suggesting the chances for mini-capsule formation is remarkably high. The obtained mini-capsules have a diameter of 1.3 ± 0.3 μm (Figure 3c). No further obvious changes were observed with prolonged sonication time.

In order to test whether electrostatic repulsion plays a role in the formation of the suprastructures, we have added NaCl electrolyte to screen this interaction during the assembly of JNPs. We have studied the JNPs' assembly in solution of 1.0 mM, 10.0 mM, and 50.0 mM NaCl. For 1.0 mM NaCl, JNPs are still capable of self-assembly, with the formation of finite structures Figure S12a. However, as the salt concentration increased to 10.0 mM, JNPs formed random aggregates without orientation. At 50.0 mM NaCl, JNPs precipitate immediately and no regular structures were observed (Figure S12c). These results indicate that the electrostatic repulsion indeed plays a role in the formation suprastructures constituted of highly oriented JNPs.

The self-assembly of JNPs under sonication conditions exhibits pronounced temperature dependence (Figure 3d). When the temperature was below 10 °C, no self-assembled structures were observed. Mini-capsules were the major aggregates when the temperature lied between 20 and 35 °C. A mixture of mini-capsules, micelles, and worms were obtained at 45 °C. Finally, micelles and worms were the only structures at 50 °C. Under such conditions, the formation and growth of micelles could be directly monitored by dynamic light scattering (DLS) (Figure 3e), indicating that the JNPs self-assembly was so efficient that the concentration of the free JNPs remained in solution was considerably low. SEM measurements show that the micelles only grow in length, without any capsule formation (Figure 3e–h). The micelle growth stopped after 5 min sonication when a maximum length around 3.0 μm was reached, which can be rationalized as excessively long micelles cannot survive from the strong shear force of sonication. It is evident that higher temperature led to stronger hydrophobic attractions,[36] which favors more stable assembled structure. In our system, micelles and worms are the most stable structures, since they expose the least hydrophobic area to aqueous solution by burying the PtBA lobes inside the core. By contrast, giant-vesicles and mini-capsules are less stable because they expose the internal hydrophobic PtBA surfaces to aqueous solution, which is energetically less favorable.

The different stability of micelles, mini-capsules, and giant-vesicles implies the potential transformation from giant-vesicles to micelles. To verify this, we exposed the giant-vesicles produced by vortex shaking (Figure 4a) to sonication at 24 °C, the same condition as the mini-capsules formation. Spherical

DOI: 10.1021/acs.jpclett.8b00206
J. Phys. Chem. Lett. 2018, 9, 1415–1421

protrusions were readily found detaching from the giant-vesicles, forming multichambered vesicles within 30 s of sonication (Figure 4b). These protrusions may originate from the wavelike domains of giant-vesicles that bulge out under shear. After 10 min of sonication, the multichambered vesicles completely disappeared with the formation of mini-capsules (Figure 4c). This observation suggests that the multichambered vesicles are very likely to be the intermediates between giant-vesicles and mini-capsules. No obvious change was observed when the sonication time was extended to 20 min. However, as the temperature rose from 24 to 50 °C with further 2 min sonication, the sizes of mini-capsules were considerably decreased from 1.4 ± 0.4 to 0.9 ± 0.2 μm with a significant increase in the micelles amount (Figure 4c,d). We thus assumed that the mini-capsules were in equilibrium with the free JNPs under sonication.

The elevated temperature efficiently assembled free JNPs into micelles and drove the disassembly of mini-capsules. This hypothesis is proved by the fact that, after another 15 min sonication, micelles and worms were the only products, viz., no mini-capsules were left (Figure 4e). Conclusions can be drawn from these observations: (*i*) supracolloidal structures stability follows the order: giant-vesicles < mini-capsules < micelles and worms, (*ii*) supracolloidal structures can be transformed from less stable to more stable states, and (*iii*) transformation from more stable to less stable suprastructures requires the disassembly of the more stable suprastructures into individual JNPs, then reassemble into targeted structures. The direct transformation from the more stable to a less stable states, i.e., from mini-capsules to giant-vesicles, was not observed in our experiments. The complete disassembly of suprastructures occurs when ethanol concentration is above 50% under sonication. A full overview of the transformation possibilities between suprastructures is depicted in Figure 4f. All the self-assembled structures are stable in quiescent solution for weeks without disassembly. It must be noted that, because of the introduction of shear forces in the current assembly system, these obtained stable suprastructures may not exist in their equilibrium state but instead are kinetically trapped in different energetic levels. To depict this idea, we qualitatively plot the relative energy states of the self-assembled structures against their activation energy barriers (Figure 4g).

In the present work, model JNPs consisting of deformable hydrophobic and rigid hydrophilic lobes were designed, synthesized, and assembled under shear conditions. The unique particle design provides a universal route to the colloidal assembly revealing supracolloidal structures with unique properties. First, such properties were mostly prevalent in molecular assembly, but were introduced into colloidal assembly in the present study. For instance, the self-assembly of the model JNPs exhibited high versatility and the supracolloidal structures showed transformable properties. Second, several unique colloidal suprastructures were discovered. Some of the newly discovered suprastructures could find molecular analogues, e.g., worms composed by anisotropic shaped colloidal particles, while others have no known molecular counterparts, such as the single-walled giant-, elongated-, and multichambered vesicles with wavelike surface structures. This is not surprising, because compared to the molecular amphiphiles, JNPs have much more rigid structure with reduced degree of freedom, being unable to adjust their conformations via chemical bond rotation during the self-assembly process, and therefore, the obtained suprastructure in the present study may be far from equilibrium. There are now many possibilities to be explored. The past decade has seen substantial growth in anisotropic colloidal particles synthesis,[9,25,26] which allows the precise control of phase separation, chemical compositions, sizes, numbers and shapes of the JNPs lobes. Independently or combined, the tuning of these parameters implies a myriad of chances to discover new supracolloidal structures and assembly properties that could be tailored for specific applications.

■ ASSOCIATED CONTENT

Supporting Information

The Supporting Information is available free of charge on the ACS Publications website at DOI: 10.1021/acs.jpclett.8b00206.

Materials, JNPs synthesis, and assembly methods, as well as Figures S1−S12 (PDF)

■ AUTHOR INFORMATION

Corresponding Author

*E-mail: andrei.honciuc@zhaw.ch.

ORCID

Chengjun Kang: 0000-0003-0208-2954

Andrei Honciuc: 0000-0003-2160-2484

Notes

The authors declare no competing financial interest.

■ ACKNOWLEDGMENTS

We thank Metrohm Foundation (Herisau, Switzerland) for financial support.

■ REFERENCES

(1) Kim, S.-H.; Lee, S. Y.; Yang, S.-M.; Yi, G.-R. Self-Assembled Colloidal Structures for Photonics. *NPG Asia Mater.* **2011**, *3*, 25−33.

(2) Yethiraj, A.; Thijssen, J. H. J.; Wouterse, A.; van Blaaderen, A. Large-Area Electric-Field-Induced Colloidal Single Crystals for Photonic Applications. *Adv. Mater.* **2004**, *16*, 596−600.

(3) Anker, J. N.; Hall, W. P.; Lyandres, O.; Shah, N. C.; Zhao, J.; Van Duyne, R. P. Biosensing with Plasmonic Nanosensors. *Nat. Mater.* **2008**, *7*, 442−453.

(4) Fenzl, C.; Hirsch, T.; Wolfbeis, O. S. Photonic Crystals for Chemical Sensing and Biosensing. *Angew. Chem., Int. Ed.* **2014**, *53*, 3318−3335.

(5) Ortel, E.; Sokolov, S.; Zielke, C.; Lauermann, I.; Selve, S.; Weh, K.; Paul, B.; Polte, J.; Kraehnert, R. Supported Mesoporous and Hierarchical Porous Pd/TiO2 Catalytic Coatings with Controlled Particle Size and Pore Structure. *Chem. Mater.* **2012**, *24*, 3828−3838.

(6) Anderson, V. J.; Lekkerkerker, H. N. W. Insights into Phase Transition Kinetics from Colloid Science. *Nature* **2002**, *416*, 811−815.

(7) Gasser, U. Crystallization in Three- and Two-Dimensional Colloidal Suspensions. *J. Phys.: Condens. Matter* **2009**, *21*, 203101.

(8) Zhang, H.; Edwards, E. W.; Wang, D.; Möhwald, H. Directing the Self-Assembly of Nanocrystals beyond Colloidal Crystallization. *Phys. Chem. Chem. Phys.* **2006**, *8*, 3288−3299.

(9) Vogel, N.; Retsch, M.; Fustin, C.-A.; del Campo, A.; Jonas, U. Advances in Colloidal Assembly: The Design of Structure and Hierarchy in Two and Three Dimensions. *Chem. Rev.* **2015**, *115*, 6265−6311.

(10) Li, F.; Josephson, D. P.; Stein, A. Colloidal Assembly: The Road from Particles to Colloidal Molecules and Crystals. *Angew. Chem., Int. Ed.* **2011**, *50*, 360−388.

(11) Whitesides, G. M.; Grzybowski, B. Self-Assembly at All Scales. *Science* **2002**, *295*, 2418−2421.

DOI: 10.1021/acs.jpclett.8b00206
J. Phys. Chem. Lett. 2018, 9, 1415−1421

(12) Glotzer, S. C.; Solomon, M. J. Anisotropy of Building Blocks and Their Assembly into Complex Structures. *Nat. Mater.* **2007**, *6*, 557−562.
(13) Mann, S. Self-Assembly and Transformation of Hybrid Nano-Objects and Nanostructures under Equilibrium and Non-Equilibrium Conditions. *Nat. Mater.* **2009**, *8*, 781−792.
(14) Liu, K.; Nie, Z.; Zhao, N.; Li, W.; Rubinstein, M.; Kumacheva, E. Step-Growth Polymerization of Inorganic Nanoparticles. *Science* **2010**, *329*, 197−200.
(15) Hu, H.; Ji, F.; Xu, Y.; Yu, J.; Liu, Q.; Chen, L.; Chen, Q.; Wen, P.; Lifshitz, Y.; Wang, Y.; et al. Reversible and Precise Self-Assembly of Janus Metal-Organosilica Nanoparticles through a Linker-Free Approach. *ACS Nano* **2016**, *10*, 7323−7330.
(16) Evers, C. H. J.; Luiken, J. A.; Bolhuis, P. G.; Kegel, W. K. Self-Assembly of Microcapsules via Colloidal Bond Hybridization and Anisotropy. *Nature* **2016**, *534*, 364−368.
(17) Kraft, D. J.; Ni, R.; Smallenburg, F.; Hermes, M.; Yoon, K.; Weitz, D. A.; van Blaaderen, A.; Groenewold, J.; Dijkstra, M.; Kegel, W. K. Surface Roughness Directed Self-Assembly of Patchy Particles into Colloidal Micelles. *Proc. Natl. Acad. Sci. U. S. A.* **2012**, *109*, 10787−10792.
(18) Skelhon, T. S.; Chen, Y.; Bon, S. A. F. Synthesis of "Hard−Soft" Janus Particles by Seeded Dispersion Polymerization. *Langmuir* **2014**, *30*, 13525−13532.
(19) Chen, Q.; Whitmer, J. K.; Jiang, S.; Bae, S. C.; Luijten, E.; Granick, S. Supracolloidal Reaction Kinetics of Janus Spheres. *Science* **2011**, *331*, 199−202.
(20) Chen, Q.; Bae, S. C.; Granick, S. Directed Self-Assembly of a Colloidal Kagome Lattice. *Nature* **2011**, *469*, 381−384.
(21) Fetsch, C.; Gaitzsch, J.; Messager, L.; Battaglia, G.; Luxenhofer, R. Self-Assembly of Amphiphilic Block Copolypeptoids − Micelles, Worms and Polymersomes. *Sci. Rep.* **2016**, *6*, 33491−39491.
(22) Cheng, X.; Jin, Y.; Fan, B.; Qi, R.; Li, H.; Fan, W. Self-Assembly of Polyurethane Phosphate Ester with Phospholipid-Like Structures: Spherical, Worm-Like Micelles, Vesicles, and Large Compound Vesicles. *ACS Macro Lett.* **2016**, *5*, 238−243.
(23) Davies, T. S.; Ketner, A. M.; Raghavan, S. R. Self-Assembly of Surfactant Vesicles That Transform into Viscoelastic Wormlike Micelles upon Heating. *J. Am. Chem. Soc.* **2006**, *128*, 6669−6675.
(24) Stuart, M. C. A.; Boekema, E. J. Two Distinct Mechanisms of Vesicle-to-Micelle and Micelle-to-Vesicle Transition Are Mediated by the Packing Parameter of Phospholipid−detergent Systems. *Biochim. Biophys. Acta, Biomembr.* **2007**, *1768*, 2681−2689.
(25) Walther, A.; Müller, A. H. E. Janus Particles: Synthesis, Self-Assembly, Physical Properties, and Applications. *Chem. Rev.* **2013**, *113*, 5194−5261.
(26) Jiang, S.; Chen, Q.; Tripathy, M.; Luijten, E.; Schweizer, K. S.; Granick, S. Janus Particle Synthesis and Assembly. *Adv. Mater.* **2010**, *22*, 1060−1071.
(27) Wu, D.; Chew, J. W.; Honciuc, A. Polarity Reversal in Homologous Series of Surfactant-Free Janus Nanoparticles: Toward the Next Generation of Amphiphiles. *Langmuir* **2016**, *32*, 6376−6386.
(28) Dreiss, C. A. Wormlike Micelles: Where Do We Stand? Recent Developments, Linear Rheology and Scattering Techniques. *Soft Matter* **2007**, *3*, 956−970.
(29) Cui, H.; Chen, Z.; Zhong, S.; Wooley, K. L.; Pochan, D. J. Block Copolymer Assembly via Kinetic Control. *Science* **2007**, *317*, 647−650.
(30) Friedrich, H.; Frederik, P. M.; de With, G.; Sommerdijk, N. A. J. M. Imaging of Self-Assembled Structures: Interpretation of TEM and Cryo-TEM Images. *Angew. Chem., Int. Ed.* **2010**, *49*, 7850−7858.
(31) Israelachvili, J. N. *Intermolecular and Surface Forces*, 3rd ed.; Academic Press: San Diego, 2011.
(32) Vazquez, G.; Alvarez, E.; Navaza, J. M. Surface Tension of Alcohol Water + Water from 20 to 50.Degree.C. *J. Chem. Eng. Data* **1995**, *40*, 611−614.
(33) Wu, S. Calculation of Interfacial Tension in Polymer Systems. *J. Polym. Sci., Part C: Polym. Symp.* **1971**, *34*, 19−30.
(34) Wu, D.; Honciuc, A. Design of Janus Nanoparticles with PH-Triggered Switchable Amphiphilicity for Interfacial Applications. *ACS Appl. Nano Mater.* **2018**, *1*, 471−482.
(35) Wu, Y. L.; Derks, D.; van Blaaderen, A.; Imhof, A. Melting and Crystallization of Colloidal Hard-Sphere Suspensions under Shear. *Proc. Natl. Acad. Sci. U. S. A.* **2009**, *106*, 10564−10569.
(36) Chandler, D. Interfaces and the Driving Force of Hydrophobic Assembly. *Nature* **2005**, *437* (7059), 640−647.

DOI: 10.1021/acs.jpclett.8b00206
J. Phys. Chem. Lett. 2018, 9, 1415−1421